Van der Waals Force Isolation of Monolayer MoS_2

*Alper Gurarslan, Shuping Jiao, Tai-De Li, Guoqing Li, Yiling Yu, Yang Gao, Elisa Riedo, Zhiping Xu, and Linyou Cao**

Van der Waals (vdW) interactions play an important role in many interfacial processes such as wetting, lubrication, adhesion, and adsorption, but the understanding has remained relatively limited. 2D materials present an unprecedented platform for the studies of interfacial vdW interactions due to the atomically thin dimension and perfect surface passivation.[1] The atomically thin dimension may allow to study interfacial vdW interactions as a function of physical features engineered with atomic-scale precision. The perfect surface passivation can ensure that the interaction at the interface is predominantly van der Waals in nature, which is difficult to realize at conventional material systems as the interfacial dangling bonds may invoke strong chemical bonding. A common strategy to study interfacial vdW interactions is to examine the process of water wetting.[2,3] Previous studies on the wetting of graphene have indicated that graphene may partially transmit the vdW interaction from the underlying substrate to the water droplet.[4–7] However, little has been known for how nongraphene 2D materials, like transition metal dichacolgenide (TMDC) materials, may affect interfacial vdW interactions. While recent studies on the wetting of 2D TMDC materials provide some useful information,[8–10] the inferior surface quality and structural uniformity of the materials used in those studies essentially prevents the possibility of precisely evaluating the interfacial vdW interaction and its correlation with physical features. For instance, it is not clear how the interfacial vdW interaction may depend on the layer number of MoS_2 and the surface properties of underlying substrates.

Here, we have demonstrated that monolayer MoS_2 can efficiently screen the vdW interaction of the underlying substrate with external systems by >90% because of the substantial increase in the physical separation between the substrate and the external systems by the presence of the monolayer. This is evidenced by a negligible dependence of the water contact angle of MoS_2 films on the layer number and on the hydrophilicity of the substrate. It is also supported by a constant vdW force between atomic force microscope (AFM) tips and the MoS_2 films with different layer numbers. The experimental observation is consistent with theoretical simulations based on an analytic model and molecular dynamic techniques. The quantitative correlation we have derived for the changes in physical separation and vdW interactions can also be generally applied to other 2D materials, such as the partial wetting transmission at graphene. Additionally, our preliminary result indicates that this efficient screening of vdW interactions by atomically thin MoS_2 monolayer bears significant implications for the dynamic control of interfacial processes.

Compared to the previous studies on the wetting of 2D TMDC materials,[9,10] in which the 2D TMDC materials used bear relatively poor surface quality and structural uniformity due to the synthetic approach, this work benefits from a unique self-limiting chemical vapor deposition technique that we developed for the synthesis centimeter-scale high-quality uniform MoS_2 films with precisely controlled layer numbers.[11] It also benefits from a surface-energy-assisted transfer technique that we developed that may perfectly transfer the synthesized film onto arbitrary substrates without compromising the quality and uniformity.[12] We have confirmed the layer number and surface roughness of all the as-grown films studied in this work, the latter of which is as low as 0.2 to 0.3 nm (Figures S1–S3, Supporting Information). We have also confirmed the high surface quality and uniformity of the transferred films (Figures S4–S6, Supporting Information). As further evidence for the superior surface quality and uniformity of our materials, the static and advancing contact angles show a difference of less than 2° (Figure S7, Supporting Information). By contrast, the wetting hysterysis is reported to be 20–30° in the previous studies.[10]

Figure 1 shows the water contact angle measured at as-grown MoS_2 films with different layer numbers on sapphire substrates. The contact angle of bare sapphire substrates is also given as a reference. To reflect the possible effect of the high-temperature synthetic process, the bare substrate was annealed under the

Dr. A. Gurarslan, G. Li, Prof. Dr. L. Cao
Department of Materials Science and Engineering
North Carolina State University
Raleigh, NC 27695, USA
E-mail: lcao2@ncsu.edu
Dr. A. Gurarslan, G. Li
Department of Fiber and Polymer Science
North Carolina State University
Raleigh, NC 27695, USA
S. Jiao, Prof. Dr. Z. Xu
Department of Mechanical Engineering
Tsinghua University
Beijing 100084, China
Dr. T.-D. Li, Y. Gao, Prof. Dr. E. Riedo
CUNY-Advanced Science Research Center
New York, NY 10031, USA
Y. Yu, Prof. Dr. L. Cao
Department of Physics
North Carolina State University
Raleigh, NC 27695, USA
Dr. T.-D. Li, Y. Gao, Prof. Dr. E. Riedo
School of Physics
Georgia Institue of Technology
Atlanta, GA 30332, USA
Prof. Dr. E. Riedo
Department of Physics
CUNY-City College of New York
New York, NY 10031, USA
Prof. Dr. E. Riedo
Phyics Program
CUNY-The Graduate Center
New York, NY 10016, USA

DOI: 10.1002/adma.201601581

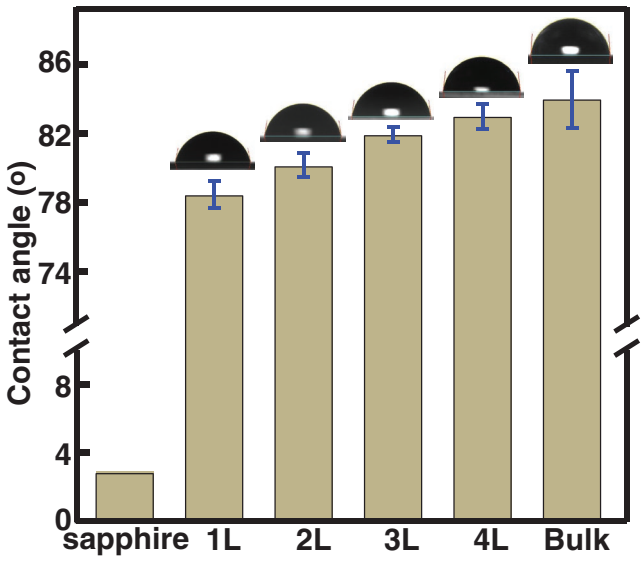

Figure 1. Mild dependence of the water contact angle of MoS_2 films on the layer number. The bar diagrams indicate the contact angles of as-grown MoS_2 films with different layer numbers on sapphire substrates. At the top of the bar the standard deviation of the measured contact angles is shown. Also given are the contact angles of bulk MoS_2 and the bare sapphire substrate. The plotted contact angle of the bare sapphire substrate does not represent the measured result, but just serves to illustrate that the contact angle is very small, <5°.

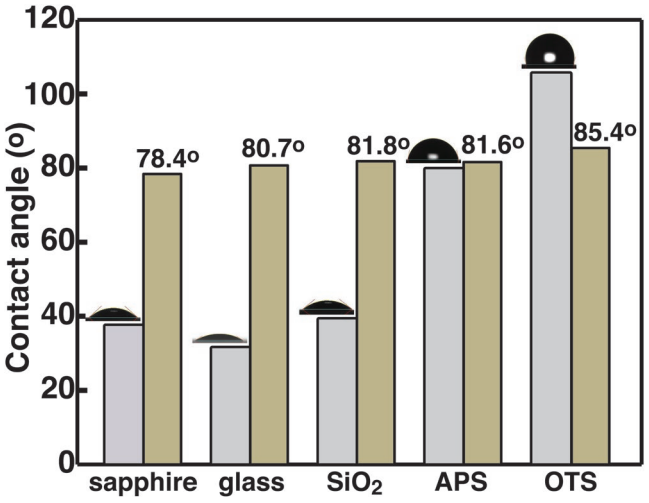

Figure 2. Minor dependence of the water contact angle of monolayer MoS_2 on the underlying substrates. The bar diagrams indicate the contact angles of the monolayer MoS_2 on different substrates (yellow) as well as the contact angles of bare substrates (grey). At the top of the bar the standard deviation of the measured contact angles of the monolayer is shown, which is usually less than 1°, and the number given is the mean value of the measured contact angle at corresponding monolayers. The substrates include sapphire (as-grown), glass, SiO_2/Si (300 nm thermally grown oxide on silicon substrates), SiO_2/Si substrates functionalized with self-assembled APTMS, and OTS.

same condition as what used for the synthesis except involving the precursors. The contact angle shows minor change with the layer number increasing, being 78.4° ± 0.8°, 80.1 ± 0.7°, 81.9°° ± 0.3°, 83.0°° ± 0.7°, and 83.9°° ± 1.6° for monolayer (1L), bilayer (2L), trilayer (3L), tetralayer (4L), and bulk MoS_2, respectively. Very interestingly, this mild layer dependence is different from what is reported with graphene.[4–7] The contact angle of graphene on hydrophilic substrates may be smaller than that of bulk graphite and increases with the layer number, which is ascribed to the capability of monolayer graphene to partially transmit the vdW interaction from the underlying substrate to the water droplet.[4–7] The minor layer-number dependence in the contact angle of MoS_2 films strongly suggests that monolayer MoS_2 may efficiently screen the interaction of the substrate with water molecules. In other words, it suggests that the wetting of the MoS_2 films is dominated by the intrinsic surface properties of MoS_2.

To further confirm the wetting screening, we transferred the synthesized centimeter-scale monolayer MoS_2 from the growth substrate (sapphire) onto other substrates, and monitored the contact angle of the transferred films as a function of the surface properties of the substrates. **Figure 2** shows the contact angles collected from the monolayer MoS_2 on different substrates, including sapphire (as-grown), glass, silicon substrates with thermally grown SiO_2 (SiO_2/Si), and SiO_2/Si substrates functionalized with self-assembled monolayers of octadecyltrichlorosilane (OTS) or 3-aminopropyltrimethoxysilane (APTMS). The contact angles of bare substrates are also plotted as reference. While the bare substrates show contact angles substantially varying from 0° to 110°, the contact angle of the supported monolayer MoS_2 maintains to be in a narrow range of 80°–86°. This again indicates that monolayer MoS_2 can efficiently screen the effect of underlying substrates in wetting, regardless of how hydrophilic the substrate is.

We can obtain quantitative understanding for the wetting screening by examining the interfacial interactions involved. According to the Young-Dupré equation, the water contact angle θ of an object is determined by the interaction potential (adhesion energy) of the object with water W versus the surface energy of water γ_w as $cos\theta = W/\gamma_w - 1$. Generally, the stronger the interaction, the smaller the contact angle. **Figure 3**a schematically illustrates the system studied in this work, in which a water droplet sits on top of monolayer MoS_2 supported by substrates. The total adhesion energy of the water droplet W_{tot} may be considered as a simple sum of the interaction potentials contributed by both the monolayer MoS_2 (W_{MoS2}) and the substrate (W_{Sub}), $W_{tot} = W_{MoS2} + W_{Sub}$.

The interaction potential (adhesion energy) contributed by the monolayer MoS_2 and the substrate may be quantitatively evaluated from water contact angles. W_{MoS2} is related with the contact angle of free-standing monolayer MoS_2 with no substrate support. While there is no way to experimentally measure the contact angle of free-standing monolayer MoS_2, we can make a reasonable estimate based on the experimental results and molecular dynamic simulation. The contact angle of free-standing monolayer MoS_2 is expected to be close to that of the monolayer on the OTS substrate, because OTS is highly hydrophobic and contributes less adhesion energy than the other substrates. Based on the experimental result, we estimate the contact angle of free-standing monolayer MoS_2 to be in the range of 85°–87°. This is also reasonably consistent with the prediction of our molecular dynamic simulations (Figures S8–S11, Supporting Information). As a result, the adhesion energy

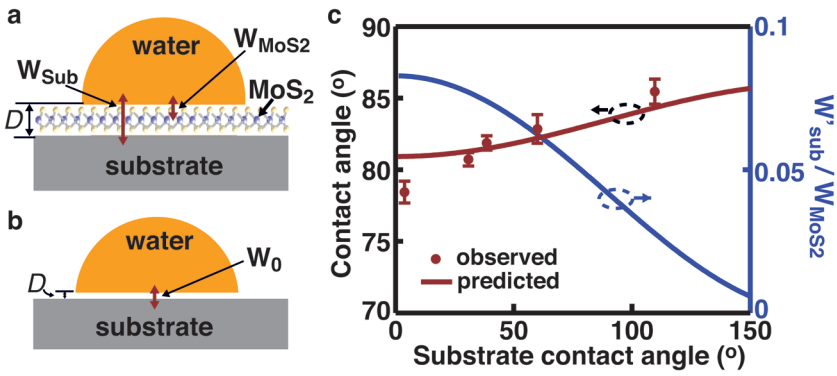

Figure 3. vdW interaction of the substrate with the water droplet. Schematic illustration for the wetting of a) monolayer MoS_2 films on substrates and b) bare substrates. The vertical red arrows indicate the vdW interactions. *D* represents the separation between the substrate and the water droplet. c) Predicted vdW interactions of the substrate with the water droplet in the presence of monolayer MoS_2 (blue curve) and contact angle of the supported monolayer as a function of the contact angle of the bare substrate. The measured contact angles of the monolayer MoS_2 on different substrates are given as red dots.

contributed by the monolayer W_{MoS2} can be estimated to be in the range of 0.0758–0.0783 J m^{-2} using the Young-Dupré equation (γ_w set to be 0.072 J m^{-2}). We can also evaluate the total adhesion energy W_{tot} from the contact angles measured at the supported monolayers, and then find out what is contributed by the substrate W_{Sub} as $W_{Sub} = W_{tot} - W_{MoS2}$. The result is given in **Table 1**. Indeed, the substrate contribution W_{Sub} only makes less than 10% of the total adhesion energy W_{tot}.

We can correlate the trivial contribution of the substrate in adhesion energy in the presence of monolayer MoS_2 to the increase in the separation between the substrate and the water. The experimental result can be nicely explained by a model based on the pairwise additivity treatment of van der Waals (vdW) interactions. According to the well-established hard-sphere model for vdW interactions, the adhesion energy can be written as a function of the separation *D* and a Hamaker constant *A* as $W = -A/(12\pi D^{[2]})$.[13] The Hamaker constant *A* is related with the density and the polarizability of the materials involved, and has been always considered to be a constant for given materials in the pairwise additivity treatment of vdW interactions.[13] The interfacial separation *D* is not the distance between neighboring atomic centers but an effective "cut-off" distance, in which the discrete and bumpy features of surface atoms are artificially "smeared out".[13] For simplicity, we can set the interfacial separation *D* to be a constant of 1.65 Å, which has been widely used as a reasonable approximation for the interfacial separation in vdW interactions.[13] The value of 1.65Å is also reasonably consistent with the prediction of our molecular dynamic simulations (Table S1, Supporting Information) and with the separations previously reported for copper-water and graphite-water systems.[5] The insertion of a MoS_2 monolayer (in thickness of 6.2 Å) may increase the substrate-water separation up to 7.85 Å. Therefore, the vdW interaction of the substrate with the water droplet in the presence of monolayer MoS_2 may dramatically decrease compared to that of the bare substrate as $W'_{Sub} = W_0$ (1.65/7.85)[2] = 0.0442 W_0, where W_0 is the vdW interaction of the bare substrate with water and can be evaluated from the bare substrate's contact angle (Figure 2). As shown in Table 1, the predicted vdW interaction of the substrate W'_{Sub} is reasonably consistent with the W_{Sub} that is derived from the experimental measurements. This consistence indicates that the wetting screening of monolayer MoS_2 is mainly due to the screening of the vdW interaction between the substrate and water as the substrate-water separation is substantially increased.

We can predict the water contact angle of monolayer MoS_2 on an arbitrary substrate using the model. The vdW interaction contributed by an arbitrary substrate underlying monolayer MoS_2 can be written as a function of the contact angle of the bare substrate θ_S as $W'_{Sub} = \gamma_w(1 + cos\theta_S)$ (1.65/7.85).[2] We can derive the water contact angle of the supported monolayer MoS_2 using $\theta = arcos[(W'_{Sub} + W_{MoS2})/\gamma_w - 1]$. The predicted contact angle θ (red curve) and vdW interaction W'_{Sub} (blue curve) are plotted as a function of the contact angle θ_S of the bare substrate in Figure 3c. The experimental results of this work are also plotted (red dots) to show the consistence between the predicted and experimental results. We can find that the predicted vdW interaction contributed by the substrate W'_{Sub} is always less than 10% of the contribution of the monolayer W_{MoS2} regardless of how hydrophilic the substrate is. We have also performed molecular dynamic simulation for the contact angle of monolayer MoS_2 supported by substrates and the simulation results confirm that the contact angle shows very mild dependence on the hydrophilicity of the substrate (Figure S9, Supporting Information).

To further illustrate the capability of monolayer MoS_2 to screen the vdW interaction of underlying substrates, we performed force-distance measurements at as-grown MoS_2 films with different layer numbers as well as bare sapphire substrates. This measurement allows us to directly evaluate the effect of MoS_2 films on the vdW interaction of underlying substrates with external systems, although the external system here is the AFM tip instead of water droplets. The force-distance curves measured by approaching the tip to the MoS_2 films are given in **Figure 4**. The maximum attractive force, which appears at "snap-in" when the tip jumps into contact with the sample, indicates the tip-sample vdW interaction when they are in touch. The interaction of the tip with the bare substrate is apparently stronger than that with the MoS_2 films. And the

Table 1. vdW interactions contributed by monolayer MoS_2 and the substrates.

	θ [°]	W_{tot} [J m^{-2}]	W_{sub} [J m^{-2}]	W'_{sub} [J m^{-2}]	W_0 [J m^{-2}]	θ [°]	Bare substrate
MoS_2/sapphire	78.4	0.0865	0.0082–0.0107	0.0064	0.1440	0	Sapphire
MoS_2/glass	80.7	0.0837	0.0054–0.0079	0.0059	0.1337	31	Glass
MoS_2/SiO_2	81.8	0.0823	0.0040–0.0065	0.0057	0.1282	38.7	SiO_2
MoS_2/APTMS	82.8	0.0811	0.0027–0.0053	0.0048	0.1077	60.3	APTMS
MoS_2/OTS	85.4	0.0782	–0.0001–0.0024	0.0021	0.0533	110	OTS

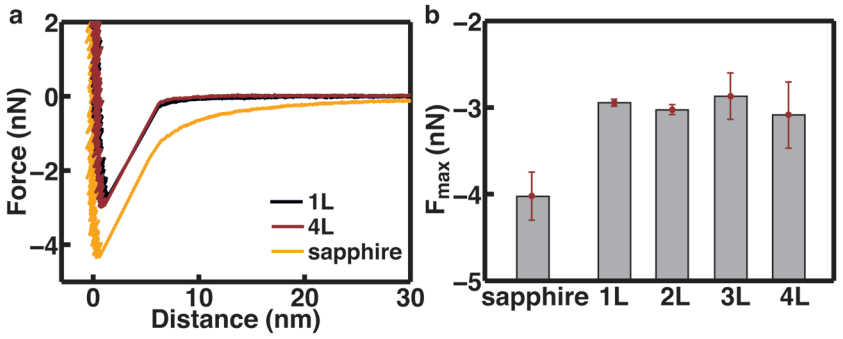

Figure 4. Force–distance relationship of the substrate with and without the presence of monolayer MoS_2. a) Measured force–distance curves for as-grown monolayer MoS_2 (black curve), tetra-layer MoS_2 (red curve), and the bare sapphire substrate (yellow curve). b) The maximum force, where the tip is in contact with the surface of the sample and corresponds to the valley in the curve given in (a) as function of the layer number of the film. At the top of the bar the standard deviation of the measured results is indicated.

interaction with the films shows negligible dependence on the layer number. This measurement provides corroborating evidence for the vdW screening of monolayer MoS_2.

As a matter of fact, we observed obvious effects of air-borne contaminants in the wetting of MoS_2, which is similar to what was previously reported for WS_2[4]. This is indicated by an increase of the contact angle with the time of being exposed to ambient environment (**Figure 5**). The adsorption of air-borne contaminant like hydrocarbon on the surface of newly made MoS_2 films has previously been confirmed by X-ray photoelectron spectroscopy and Auger electron spectroscopy.[14] However, the effect of the air-borne contamination does not affect our conclusion and analysis for the vdW screening. The contact angles of freshly made MoS_2 films or newly cleaved bulk MoS_2 materials show minor dependence on the layer number as well, all in the range of 65–69° (Figure 5 inset). This indicates that the wetting isolation is intrinsic to monolayer MoS_2, instead of the effect of air-borne contamination. Additionally, we did not observe any substantial change in the surface smoothness and thickness of the film with the exposure time with AFM and elliposometry measurements (Figures S12,S13, Supporting Information). Previous studies demonstrated that the air-borne contaminant adsorbed on SiO_2 surfaces might be in thickness of only 1–2 Å.[15] Given the lower surface energy of MoS_2, the air-borne contaminant on our materials is expected to be even less and thus might be difficult to be convincingly resolved by AFM and ellipsometry measurements. Therefore, the increase in the substrate-water separation is mainly dictated by the thickness of the monolayer MoS_2 even with the presence of adsorbed air-borne contaminants.

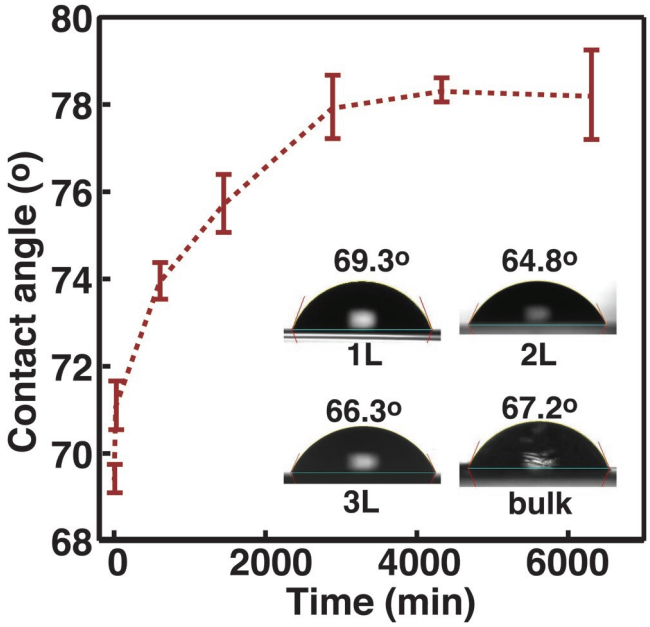

Figure 5. Evolution of the contact angle of as-grown monolayer MoS_2 as a function of the exposure time to ambient environment. The time is counted starting from when the monolayer is taken out of the synthetic setup. Insets are the images for the contact angle measured at MoS_2 films and bulk MoS_2 materials with exposure time less than 5 min.

The difference between the wetting isolation of monolayer MoS_2 and the partial wetting transmission previously reported with graphene can be correlated to the different thickness of the two materials. Monolayer graphene is reportedly able to partially transmit the vdW interaction of underlying substrates as its contact angle is subject to the strong influence of the substrate.[4–7] We can perform similar analysis for graphene as what we did for monolayer MoS_2 (for details see the Supporting Information). As the measured contact angles for graphene vary substantially in the literature.[4–7,16] here we focus on analyzing the results measured at freshly made graphene and newly cleaved highly ordered pyrolytic graphic (HOPG).[4] The contact angles are 51°, 59°, and 64° for fresh monolayer graphene on copper, —two to three layer graphene on nickel, and newly cleaved HOPG, respectively.[4] From the observed contact angles, the vdW interaction contributed by the copper substrate W_{Sub} can be estimated to be 0.0248 J m^{-2}. By contrast, the counterpart W'_{Sub} is predicted to be 0.0154 J m^{-2} by considering the effect of increased separation (from 1.65 to 5.05 Å). By the same token, the observed and predicted vdW interactions from the nickel substrate in the 2–3 layer grpahene grown on nickel can be found to be 0.0038 J m^{-2} and 0.0028–0.0055 J m^{-2}, respectively. The reasonable consistence between W_{Sub} and W'_{Sub} suggests that, similar to monolayer MoS_2, the role of graphene is just increasing the substrate-water separation. The partial wetting transmission at monolayer graphene reported in previous studies is simply because graphene may not increase the substrate-water separation as much as monolayer MoS_2 due to its smaller thickness (3.4 Å vs 6.2 Å).

In conclusion, we have demonstrated that monolayer MoS_2 can efficiently screen the vdW interaction from the underlying substrates to external systems by >90 due to the substantial increase in the separation between the substrate and the external system by the presence of the MoS_2 monolayer. This means that the wettability of an object covered by MoS_2

monolayer is dominated by the intrinsic surface properties of the monolayer. As monolayer MoS_2 also features with excellent electrical, optical, and catalytic properties,[17–20] its dominance in interfacial vdW interactions may enable capabilities to dynamically manipulate the interfacial process through electrical, optical, or chemical ways. For instance, we have observed that the contact angle of monolayer MoS_2 can be tuned by applying a gating voltage (Figure S14, Supporting Information).

Experimental Section

Synthesis, Transfer, and Characterization of Centimeter-Scale MoS_2 Films: The centimeter monolayer and fewlayer MoS_2 films were grown using a chemical vapor deposition process in a tube furnace that we have previously reported.[11] Molybdenum chloride ($MoCl_5$) (99.99%, Sigma-Aldrich) and sulfur powder (Sigma-Aldrich) were used as precursors and sapphire as growth substrates. Typical conditions for high-quality MoS_2 thin film growth include a temperature of 850 °C and a pressure around 2 Torr. The layer number was controlled by controlling the amount of precursors ($MoCl_5$) used in the synthesis.

The transfer of the synthesized film was performed using a surface-energy-assisted transfer process that we have previously developed.[12] This process leverages on the different surface properties of MoS_2 films and the growth substrates. Basically, a layer of polystyrene (PS) was spin coated on as-grown MoS_2 films, followed by dropping a water droplet on the top. Driven by the different surface energies of the hydrophobic MoS_2 film and the hydrophilic substrate, water molecules could penetrate underneath the MoS_2 film to lift the film off the growth substrate. After removing the water droplet with paper towel, we could pick up the assembly with a pair of tweezers and transferred onto target substrate. The PS was removed by rinsing with toluene several times.

The uniformity, layer number, and crystalline quality of the as-grown and transferred MoS_2 were characterized by a variety of tools, including atomic force microscope (AFM, Veeco Dimension-3000), Raman spectroscope (Renishaw-1000), and optical microscope.

Contact Angle Measurements of Centimeter-Scale MoS_2 Films: The contact angle measurements were conducted on a First Ten Angstroms (FTA) 1000 C Class goniometer equipped with a dispensing needle and an HD camcorder (Canon VIXIA HF S20) mounted on a microscope (Olympus SZ-61l). 1 µL deionized water droplet generated with the automatic dispenser was gently brought in contact with the sample surface and then a snapshot was taken after separating the droplet from the needle for the static contact angle. Then static contact angle calculated from the tangent of the water droplet at the intersection of the air/drop surface using the spherical fit option on the FTA 32 software. For advancing and receding contact angles measurements, water droplet was placed on the sample surface and the volume of the droplet increased and then decreased gradually.

Force-Distance Measurements of As-Grown MoS_2 Films: The force-distance measurements were performed with a Multimode AFM while approaching a conductive tip to MoS_2 films deposited on double side-polished sapphire samples. The humidity was controlled and kept at 38–40%. A conductive tip (Pt/Ir) attached to a cantilever with force constant of 0.49 N m^{-1} was used. For each sample different measurements on three different positions were repeated, showing reproducibility of the data. The data were acquired with a scanner z-range of 100 nm at approaching speeds of 20 nm s^{-1}. Only the range 3–30 nm is shown because the force at longer distances doesn't show any variation. The MoS_2 films are grounded with cooper double side tape that will ground the substrate from the bottom side of the sample. Around the edges of the sample, a silver paste that grounds the MoS_2 layers on top of the substrate is used. For the calibration of the spring constant and force-distance curves see previous works.[21,22]

Molecular Dynamics Simulations: MD simulations were carried out by using the large-scale atomic/molecular massively parallel simulator. All equilibrium simulations were performed at a constant temperature of 300 K by using the Nosé-Hoover thermostat. The time step for integrating equations of motion was set to be 1 fs. The rigid SPC/E model was used for water molecules. The SHAKE algorithm was applied for the stretching terms between oxygen and hydrogen atoms to reduce high-frequency vibrations that require a shorter time step for numerical integration. The interaction between water and MOS_2 includes both van der Waals and electrostatic terms and the parameters are listed in the Table S1 (Supporting Information), which are taken from Ref. [2]. The van der Waals forces calculated in the Lennard-Jones 12–6 form $V(r) = 4\varepsilon[(\sigma/r)^{12} - (\sigma/r)^6]$ are truncated at 2.0 nm, and the long-range Coulomb interactions are computed by using the particle–particle particle-mesh algorithm with an accuracy of 10^{-4}. A droplet consisting of 1588 water molecules was involved in the simulation. More detailed information about the MD simulation can be found in the Supporting Information.

Supporting Information

Supporting Information is available from the Wiley Online Library or from the author.

Acknowledgements

The synthesis and transfer work was supported by a Young Investigator Award from the Army Research Office (W911NF-13-1-0201). The work of contact angle measurement, data analysis, and theoretical modeling was supported part of the Center for the Computational Design of Functional Layered Materials, an Energy Frontier Research Center funded by the U.S. Department of Energy, Office of Science, Basic Energy Sciences under Award # DE-SC0012575. E. R., T.-D. L., and Y. G. performed the AFM measurement and thank the support of the Office of Basic Energy Sciences of the Department of Energy (DE 0000224414). The authors thank D. Brenner, E. Reed, and J. Miller for useful discussion, and M. Dickey for providing access to the goniometer, and acknowledge the use of the Analytical Instrumentation Facility (AIF) at North Carolina State University, which is supported by the State of North Carolina and the National Science Foundation.

Received: March 22, 2016
Revised: July 7, 2016
Published online: September 30, 2016

[1] S. Z. Butler, S. M. Hollen, L. Cao, Y. Cui, J. A. Gupta, H. R. Gutierrez, T. F. Heinz, S. S. Hong, J. Huang, A. F. Ismach, E. Johnston-Halperin, M. Kuno, V. V. Plashnitsa, R. D. Robinson, R. S. Ruolff, S. Salahuddin, J. Shan, L. Shi, M. G. Spencer, M. Terrones, W. Windl, J. E. Goldberger, *ACS Nano* **2013**, *7*, 2898.
[2] D. Bonn, J. Eggers, J. Indekeu, J. Meunier, E. Rolley, *Rev. Mod. Phys.* **2009**, *81*, 739.
[3] P. G. de Gennes, *Rev. Mod. Phys.* **1985**, *57*, 827.
[4] Z. Li, Y. Wang, A. Kozbial, G. Shenoy, F. Zhou, R. McGinley, P. Ireland, B. Morganstein, A. Kunkel, S. P. Surwade, L. Li, H. Liu, *Nat. Mater.* **2013**, *12*, 925.
[5] J. Rafiee, X. Mi, H. Gullapalli, A. V. Thomas, F. Yavari, Y. Shi, P. M. Ajayan, N. A. Koratkar, *Nat. Mater.* **2012**, *11*, 217.
[6] C. J. Shih, M. S. Strano, D. Blankschtein, *Nat. Mater.* **2013**, *12*, 866.
[7] C. J. Shih, Q. H. Wang, S. Lin, K. C. Park, Z. Jin, M. S. Strano, D. Blankschtein, *Phys. Rev. Lett.* **2012**, *109*, 176101.
[8] A. Kozbial, X. Gong, H. Liu, L. Li, *Langmuir* **2015**, *31*, 8429.
[9] A. P. S. Gaur, S. Sahoo, M. Ahmadi, M. J. Guinel, R. S. Katiyar, *Nano Lett.* **2014**, *14*, 4314.
[10] P. K. Chow, E. Singh, B. C. Viana, J. Gao, J. Luo, J. Lin, A. L. Elias, Y. Shi, Z. Wang, M. Terrones, N. Koratkar, *ACS Nano* **2015**, *9*, 3023.

[11] Y. Yu, Y. C. Li, Y. Liu, L. Su, Y. Zhang, L. Cao, *Sci. Rep.* **2013**, *3*, 1866.
[12] A. Gurarslan, Y. Yu, L. Su, Y. Yu, F. Suarez, S. Yao, Y. Zhu, M. Ozturk, Y. Zhang, L. Cao, *ACS Nano* **2014**, *8*, 11522.
[13] J. N. Israelachvili, *Intermolecular and Surface Forces*, 3rd Ed., Academic Press, San Diego, CA, USA **2011**.
[14] K. Miyoshi, *Solid Lubrication Fundamentals and Applications*, Marcel Dekker, New York, NY, USA **2001**.
[15] A. Shinozaki, K. Arima, M. Morita, I. Kojima, Y. Azuma, *Anal. Sci.* **2003**, *19*, 1557.
[16] R. Raj, S. C. Maroo, E. N. Wang, *Nano Lett.* **2013**, *13*, 1509.
[17] Q. H. Wang, K. Kalantar-Zadeh, A. Kis, J. N. Coleman, M. S. Strano, *Nat. Nanotech.* **2012**, *7*, 699.
[18] M. Chhowalla, H. S. Shin, G. Eda, L. J. Li, K. P. Loh, H. Zhang, *Nat. Chem.* **2013**, *5*, 263.
[19] Y. Li, Y. Yu, Y. Huang, R. A. Nielsen, W. A. Goddard III, Y. Li, L. Cao, *ACS Catal.* **2015**, *5*, 448.
[20] Y. Yu, S.-Y. Huang, Y. Li, S. N. Steinmann, W. Yang, L. Cao, *Nano Lett.* **2014**, *14*, 553.
[21] D. Ortiz-Young, H.-C. Chiu, S. Kim, K. Voïtchovsky, E. Riedo, *Nat. Commun.* **2013**, *4*, 2482.
[22] H. C. Chiu, D. Ortiz-Young, E. Riedo, *Rev. Sci. Instrum.* **2014**, *85*, 123707.